Side Wall Coupling Via-Hole Array Cavity Band-Pass Filter

R. B. Hwang

Department of Communication Engineering, National Chiao Tung University
1001, Ta-Hsueh Road, Hsinchu, Taiwan, R.O.C.
Email: raybeam@mail.nctu.edu.tw

ABSTRACT: In this paper, we present a substrate integrated waveguide-based band-pass filter with wide stop-band rejection property. This band-pass filter is made up of two substrate integrated waveguide cavities, which couple to each other by an aperture on their common waveguide side wall. We employed the rigorous mode-matching method to analyze the electromagnetic boundary-value problem of the structure containing multiple discontinuities. In comparison with the conventional end-to-end coupled cavity filters, we found that our new side-wall-coupled cavity filter can suppress the second resonance frequency and, therefore, provide a considerably wide rejection band. It is interesting to note that the suppression of the second resonance frequency can be achieved by properly shifting the second cavity in lateral direction.

Index Terms—band-pass filter, cavity, substrate integrated waveguide, resonator, periodic structures

INTRODUCTION

Recently, the post-wall waveguide technique or the substrate integrated waveguide technique [1-10], was developed to fabricate an equivalent rectangular metallic waveguide on a low-loss microwave substrate. Such a class of waveguides has been proved [9] to be able to preserve the well-known advantages of conventional closed rectangular waveguide, such as high-Q factor. Besides, the substrate integrated waveguide is based on printed circuit board fabrication process; therefore, it is easy to be integrated with the micro-strip, coplanar waveguide, or the other planar circuits, to design a microwave/millimeter wave sub-system. In addition to the substrate integrated waveguide, the cavity based on the substrate integrated waveguide technology was also well developed [10]. The novel substrate integrated waveguide cavity filter with defected ground structure was investigated to provide a high stop-band rejection and low insertion loss.

In this paper, we designed a band-pass filter using two coupled substrate integrated waveguide-based cavities, which are coupling to each other by an aperture on their common side wall. By following the design criterion and empirical formula [9], we could have the equivalent closed rectangular waveguide structure parameters. Moreover, the rigorous mode-matching method is employed to convert the 2-D electromagnetic boundary-value problem into a transmission line network including transformer-bank-like input-output relation at the discontinuity. The transmission and reflection characteristics, and electromagnetic fields distribution, as well, in the substrate integrated waveguide cavities were determined.

As is well known for the conventional end-to-end coupled cavity filter, the second resonant mode provides an extra pass-band. For some practical application, the second pass-band is undesired. To have a band-pass filter with high rejection for the second pass-band, we have offset the second cavity to reduce the aperture coupling. We have fabricated and measured the band-pass filter for verifying the design concept. The good agreement between the measured and calculated results validates the design concept and theoretical analysis model. Besides, the physical mechanism of high stop-band rejection for the second resonant mode was clearly interpreted by inspecting theoretically the contour map of the electric field combined with the simple coupled-mode theory.

DESCRIPTION OF THE PROBLEM

Figure 1(a) depicts a conventional end-to-end coupled cavities filter, where the cavity was made by post-wall (or via-hole) waveguide techniques. Such a type of cavity filter has been developed and applied in microwave system [10]. In this paper, we developed a cavity filter, shown in Figure 1(b) and 1(c), consisting of two post-wall-based cavities couple to each other through an aperture on their common waveguide side wall. Each of the waveguide connects with a micro-strip line with taper at its end, shown in figure 1(c). The widths of the two waveguides are h1 and h2, respectively. The widths of the inductive irises in the input and output waveguide are, a1 and a2, respectively. The width of the coupling aperture on the common sidewall of the two waveguides is w. The distances from the inductive irises to the front end of the coupling aperture are l1 and l2, respectively, in the input and output waveguide. The distance from the short circuit board to the aperture are designated as l3 and l4 in the two waveguides. The waveguide wall is implemented by placing periodic metallic via-holes with considerably small distance between adjacent holes. To maintain the waves guided in the waveguide and simultaneously reduce the power leakage, we have followed the criterion reported in the literature [9, 10] to design the substrate integrated waveguide.

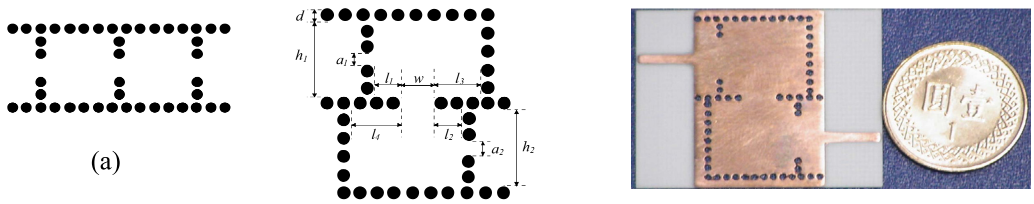

(a) (b) (c)

Figure 1: Structure configuration

METHOD OF ANALYSIS

There are many numerical methods well developed for resolving the electric and magnetic fields in the substrate integrated waveguide. To mention a few, the finite-difference frequency-domain algorithm incorporating the perfect matched layer was developed [10] to discretize the continuous spectrum, and thus the resonance frequency and Q-factor can be obtained by solving a standard matrix eigen-value problem [10]. The finite-element method was also developed to analyze the guided-wave and leaky-wave characteristics of a substrate integrated waveguide [9]. In this paper, we employed the rigorous mode-matching method to deal with the electromagnetic boundary-value problem. Firstly, for simplifying the mathematical analysis, we have used the accurate empirical equation for determining the equivalent rectangular waveguide width w_{eff}, which is given as follow

$$w_{eff} = w - 1.08\left(d^2/s\right) + 0.1\left(d^2/w\right). \qquad (1)$$

Where d and s are the diameter and the period of the metallic via-holes, and w is the distance between two via-hole walls (center-to-center). As indicated in [18], when s/d is smaller than three and d/w is smaller than 1/5, the empirical formula is very accurate. We followed the guideline and criterion given previously to design the waveguide; therefore, the equivalent rectangular waveguide can be determined to model the via-holes waveguide. Furthermore, because that the thickness of the substrate is much smaller compared with the width and length, there exists three field components, i.e., E_z, H_x and H_y. The E_z component is assumed to be invariant along the z-axis. Therefore, the problem can be simplified to a two-dimensional (2-D) boundary-value problem. The mode-matching method was well developed and widely applied in solving the electromagnetic problem with canonical structure, such as rectangular and circular cylindrical waveguides, because that the eigen-mode has close-form solution in those structures. Since the structure under consideration consists of many simple rectangular waveguides and discontinuity structures, the mode-matching method was then used to deal with electromagnetic field problem. In the following section, we will briefly introduce the mathematical procedure for solving the electromagnetic fields in the structure; however, the detail mathematical derivation and procedure could be found in the literature.

NUMERICAL AND EXPERIMENTAL RESULTS

Based on the mathematical formulation mentioned earlier, we have developed a computer program to calculate the electric and magnetic fields distribution in the structure, as well as the scattering parameters, such as return- and insertion-loss at the input and output ports, respectively. Although not shown here, we have carefully examined the numerical convergence against the number of waveguide modes employed, and the field continuity at the discontinuities, as well. In addition to the numerical simulation, we have carried out the experimental studies by fabricating the printed waveguide on the microwave substrate Rogers RO4003 with thickness 20mil. The metallic via-hole, connecting the top and bottom metal plates, was implemented by electroplating technique to ensure a good electrical performance. The period of via holes is 1.4mm. The distance between two adjacent via holes is 0.4mm. The S-parameters were measured using vector network analyzer (VNA) HP-8722D, and the universal test fixture Anritsu 3680K employed for reducing the loss due to SMA connector.

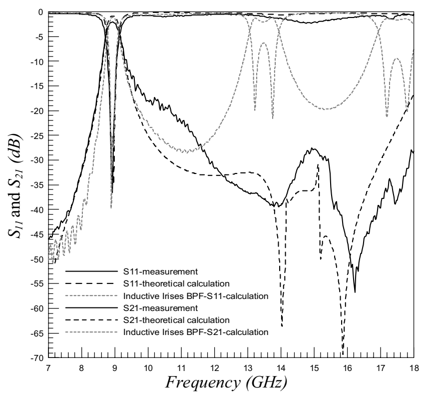

Figure 2: Insertion- and return- loss of the band-pass filter; the geometric parameters are: $h_1=h_2$=11mm, $l_1=l_2$=2.5, $l_3=l_4$=4.12mm, w=4.3mm, $tg_1=tg_2$=1mm, $a_1=a_2$=6.2mm, tm=1mm.

Figure 2 depicts the return loss and insertion loss of the band-pass filter, shown in figure 1(b) and 1(c), developed in this paper. Besides, substrate-integrated-waveguide-based end-to-end coupled cavity filter, shown in figure 1(a), was demonstrated to compare their performance. The black and long dashed lines in this figure represent the calculated return- and insertion- loss, while the solid lines stand for the measured ones. The gray and short dashed lines are the calculated return- and insertion- loss of the end-to-end coupled band-pass filter. In this example, the windows of the inductive irises are the same for the two band-pass filters. Besides, all the cavities share the same dimensions. From this figure, it is apparently to see a good agreement between the calculated and measured S-parameters. This may confirm the accuracy of the theoretical analysis model developed in this paper. It is noted that in this figure the end-to-end coupled cavity filter has a second pass band around 13.5GHz. On the contrary, the band-pass filter developed in this paper can suppress this resonant mode. In fact, the pass-band frequency can be roughly estimated by the resonance frequency of the waveguide cavity; for instance, the resonance wavelength of the cavity resonant modes TM_{mn0} is given below

$$\lambda_{mn} = 2\sqrt{\varepsilon_s} / \sqrt{(m/a)^2 + (n/b)^2} \, . \tag{2}$$

The indices m, n and 0 denote the mode number along the width-, length- and thickness- direction, respectively. Since the thickness of the waveguide is much smaller compared with the width and length, the index number is set to be zero. It is obviously to see that the pass band around 9GHz corresponds to the TM_{110} resonant mode, while the second pass band, taking place around 13.5GHz corresponding to that of TM_{120} resonant mode. However, the second pass band disappears in the side wall aperture coupling band-pass filter case. In the following numerical example, we will explain this phenomenon by investigating the electric field distribution in the two coupled cavities.

We have also carried out numerical simulations and experimental studies for such a type of band-pass filters with different aperture widths. In this example, we fabricated four samples with the aperture width w = 3.9 mm, 4.1 mm, and 4.5 mm (the cavity dimensions and structural configuration remain), and measured their transmission and reflection characteristics, as shown in figure 3(a), (b), and (c), respectively. The solid lines in each figure represent the measured results, while the dashed lines are those of calculated results. From these results, we found a good agreement between the calculated and measured results for each case. As is well known in coupled-mode theory, if the two cavities are coupling to each other, the resonant frequency of the single cavity separates into two distinct frequencies. The amount of the separation in frequency determines the coupling coefficient of the two-cavity system, which is specified by the mathematical formula given below

$$c = \left(f_u^2 - f_l^2\right) / \left(f_u^2 + f_l^2\right). \tag{3}$$

Where f_u and f_l represent the upper and lower resonant frequencies, respectively. Moreover, if the width of the coupling aperture is small, from the physics intuition we know that the coupling coefficient is not considerable; thus, it means that the two resonant frequencies are close to each other. As we gradually increase the aperture width, the separation of the two resonant frequencies becomes wider and the coupling coefficient becomes stronger accordingly. This phenomenon can be confirmed by observing figure 3(c); the increase in the aperture width indeed increases the separation between the two resonant frequencies and also broadens the pass-band bandwidth. Notice that the increase in the aperture width shall lower the pass-band frequency.

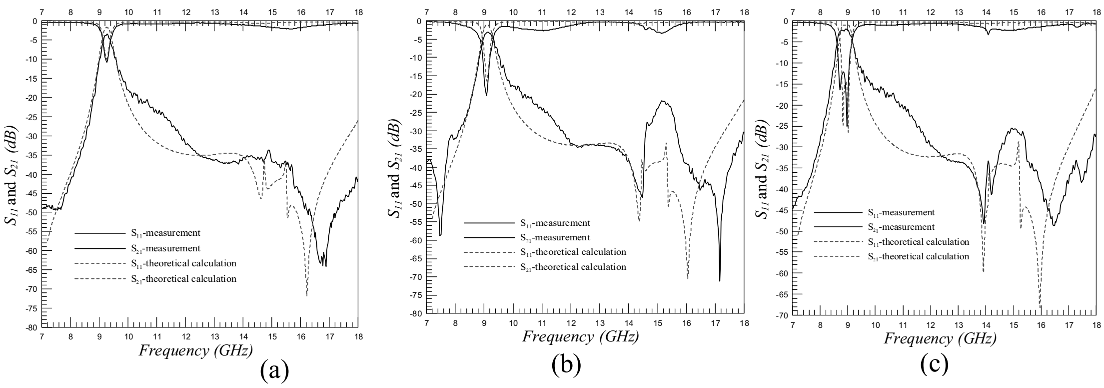

Figure 3: Insertion- and return- loss against frequency for the band-pass filters, developed in this paper, with various aperture widths (the cavity dimensions and structural configuration remain); (a) $w = 3.9mm$, (b) $w = 4.1mm$, (c) $w = 4.5mm$ and (d) $w = 4.7mm$, respectively.

CONCLUSION

In this paper, a band-pass filter made up of two substrate-integrated-waveguide-based cavities coupled by an aperture on their common side wall was investigated theoretically and experimentally. The theoretical analysis using the rigorous mode-matching method incorporating the transmission line representation was employed to calculate the reflection and transmission characteristics, as well as the electric fields distribution. It is interesting to note that by shifting the position of the second cavity in the lateral direction, the second resonant mode is greatly suppressed, and thus provide a high stop-band rejection for this harmonic. This concept was verified by theoretically inspecting the electric fields distribution in the two-cavity system. The good agreement between the calculated and measured results confirms the theoretical formation. Besides, such a band-pass filter design can provide a low insertion loss around 9GHz, and a high rejection for the second pass-band. It may be a promising design in realizing a low-cost printed circuit based waveguide filter design.

REFERENCES

[1] D. Deslandes and K. Wu, ‘‘Single-substrate integration technique of planar circuits and waveguide filters,’’ *IEEE Trans. Microw. Theory Tech.*, vol. 51, no. 2, pp. 593–596, Feb. 2003.

[2] D. Deslandes and K. Wu, ‘‘Integrated microstrip and rectangular waveguide in planar form,’’ *IEEE Microw. Wireless Compon. Lett.*, vol. 11, no. 2, pp. 68–70, Feb. 2001.

[3] Y. Cassivi, L. Perregrini, P. Arcioni, M. Bressan, K. Wu, and G. Conciauro, ‘‘Dispersion characteristics of substrate integrated rectangular waveguide,’’ *IEEE Microw. Wireless Compon. Lett.*, vol. 12, no. 9, pp. 333–335, Sep. 2002.

[4] Y. Cassivi and K.Wu, ‘‘Low cost microwave oscillator using substrate integrated waveguide cavity,’’ *IEEE Microw. Wireless Compon. Lett.*, vol. 13, no. 2, pp. 48–50, Feb. 2003.

[5] F. Xu,Y. L. Zhang,W. Hong, K.Wu, and T. J. Cui, ‘‘Finite-difference frequency- domain algorithm for modeling guided-wave properties of substrate integrated waveguide,’’ *IEEE Trans. Microw. Theory Tech.*, vol. 51, no. 11, pp. 2221–2227, Nov. 2003.

[6] H. Li,W. Hong, T. J. Cui, K.Wu, Y. L. Zhang, and L. Yan, ‘‘Propagation characteristics of substrate integrated waveguides based on LTCC,’’ in *IEEE MTT-S Int. Microwave Symp. Dig.*, Philadelphia, PA, 2003, pp. 2045–2048.

[7] Y. Huang, K. L. Wu, and M. Ehlert, ‘‘An integrated LTCC laminated waveguide-to-microstrip line T-junction,’’ *IEEE Microw. Wireless Compon. Lett.*, vol. 13, no. 8, pp. 338–339, Aug. 2003.

[8] Z. C. Hao,W. Hong, X. P. Chen, J. X. Chen, K.Wu, and T. J. Cui, ‘‘Multilayered substrate integrated waveguide (MSUBSTRATE INTEGRATED WAVEGUIDE) elliptic filter,’’ *IEEE Microw. Wireless Compon. Lett.*, vol. 15, no. 2, pp. 95–97, Feb. 2005.

[9] Feng Xu and Ke Wu, ‘‘Guided-Wave and Leakage Characteristics of Substrate Integrated Waveguide,’’ *IEEE Trans. Microw. Theory Tech.*, vol. 53, no. 1, pp.66–73, Jan. 2005.

[10] Yu Lin Zhang, Wei Hong, Ke Wu, Ji Xin, Chen and Hong Jun Tang, ‘‘Novel Substrate Integrated Wavegudide Cavity Filter with Defected Ground Structure,’’ *IEEE Trans. Microw. Theory Tech.*, vol. 53, no. 4, pp.1280–1287, April. 2005.